STATISTICS, OPTIMIZATION AND INFORMATION COMPUTING
Stat., Optim. Inf. Comput., Vol. **14**, November 2025, pp 0–17.
Published online in International Academic Press (www.IAPress.org)

Novel Hybrid Conjugate Gradient Technique Based on the Newton Direction Applied to Image Restoration Problem

Romaissa Mellal [1,*], Nabil Sellami [1], Basim A. Hassan [2]

[1] *Laboratory of ACED, Department of Mathematics, 8th May 1945 Univ., Guelma, Algeria*
[2] *College of Computer Science and Mathematics, Univ. of Mosul, Mosul, Iraq*

Abstract We introduce a novel hybrid conjugate gradient method for unconstrained optimization, combining the AlBayati-AlAssady and Rivaie-Mustafa-Ismail-Leong approaches, where the convex combination parameter is determined to ensure alignment between the conjugate gradient direction and the Newton direction. Through rigorous theoretical analysis, we establish that the proposed method guarantees sufficient descent properties and achieves global convergence under the strong Wolfe line search conditions. Numerical results confirm that, using the performance profile of Dolan and Moré, our method, denoted as hnBARMIL, consistently outperforms classical conjugate gradient methods, particularly for large-scale problems. Furthermore, we demonstrate the practical utility of our method through application to image restoration problems, where hnBARMIL exhibits competitive or superior performance compared to the Fletcher-Reeves algorithm, especially when processing images with higher noise levels.

Keywords Nonlinear Conjugate Gradient, Unconstrained Optimization, Strong Wolfe Line Search, Image Restoration Problems.

AMS 2010 subject classifications 90C26, 90C30, 65K05, 49M37.

DOI: 10.19139/soic-2310-5070-2897

1. Introduction

Optimization problems in image restoration affected by impulse noise present significant challenges due to the nonsmooth and complex nature of their objective functions. Traditional gradient-based methods often fail to address these issues effectively. Thanks to recent progress in optimization, noise removal algorithms have become more powerful and dependable. Performance assessments of gradient-based and conjugate gradient techniques for image denoising and restoration are detailed in [11, 12].
The nonlinear conjugate gradient method (CGM) is widely used for large-scale unconstrained optimization due to its simplicity, low memory requirements, and efficiency. CGM methods have thus become essential not only in image restoration [8, 23, 24, 25, 27, 28, 30] but also in scientific and engineering fields such as signal reconstruction, parameter estimation, portfolio optimization, and robotics [4, 22].
Consider the following unconstrained optimization problem:

$$\min_{u\in\mathbb{R}^n} \mathcal{G}(u). \tag{1}$$

where $\mathcal{G}:\mathbb{R}^n\to\mathbb{R}$ belongs to class $\mathcal{C}^1$.
To solve (1) using the CGM, we generate an iterative sequence of the form:

$$u_{k+1} = u_k + \lambda_k d_k, \tag{2}$$

*Correspondence to: Romaissa Mellal (Email: romaissa.mellal@yahoo.fr).Laboratory of ACED, Department of Mathematics, 8th May 1945 Univ., Guelma, Algeria.

ISSN 2310-5070 (online) ISSN 2311-004X (print)

where u_k is the current iterate and λ_k is the step length determined by a line search along the direction d_k, defined as:

$$d_k = \begin{cases} -q_k, \text{ for } k = 1, \\ -q_k + \beta_k d_{k-1}, \text{ for } k \geq 2, \end{cases} . \tag{3}$$

where $q_k = \nabla \mathcal{G}(u_k)$, and the scalar parameter β_k is chosen to ensure that d_k constitutes the k^{th} conjugate direction, assuming the objective function is quadratic and the line search is exact [6]. The performance of a CGM critically depends on its update parameter β_k, which determines the search direction by combining current gradient information with the previous search direction.
The first nonlinear CG variant introduced was the FR CGM [19], it is an extension of the HS CGM [26] which was proposed for the linear case. Many other CGMs have been proposed we cite PRP [35, 36], CD [18], LS [31], DY [14] and WYL [43]. Their formulas for β_k are given by :

$$\begin{aligned} &\beta_k^{HS} = \frac{q_{k+1}^T y_k}{d_k^T y_k}, \ \beta_k^{FR} = \frac{||q_{k+1}||^2}{||q_k||^2}, \ \beta_k^{PRP} = \frac{q_{k+1}^T y_k}{\|q_k\|^2}, \ \beta_k^{CD} = \frac{-||q_{k+1}||^2}{q_k^T d_k}, \\ &\beta_k^{LS} = \frac{-q_{k+1}^T y_k}{q_k^T d_k}, \ \beta_k^{DY} = \frac{\|q_{k+1}\|^2}{d_k^T y_k}, \ \beta_k^{WYL} = \frac{q_{k+1}^T \left(q_{k+1} - \frac{|q_{k+1}|}{|q_k|} q_k \right)}{|q_k|^2}. \end{aligned} \tag{4}$$

where $y_k = q_{k+1} - q_k$ represents the gradient difference.
In 1986, AlBayati- AlAssady [2] proposed a new variant :

$$\beta_k^{BA} = \frac{||y_k||^2}{d_k^T y_k}, \ AlBayati - AlAssady \tag{5}$$

In 2010, AlBayati et al. [3], proposed a modification of the BA method. This approach produces a direction parallel to the search direction given by the HS algorithm for quadratic functions.
After that, in 2012, Rivaie et al. [38] introduced a novel variant of CGM, designated as the RMIL method.
This approach is a modification of the PRP method, with the variant given by the following formula:

$$\beta_k^{RMIL} = \frac{q_{k+1}^T y_k}{\| d_k \|^2}. \ Rivaie - Mustafa - Ismail - Leong \tag{6}$$

Note that, the RMIL variant is not necessarily negative.
In 2015 and 2016, M. Rivaie et al. [39] and Dai [13] proposed a modified version of the RMIL method, further enhancing its robustness and global convergence. Other modification were proposed, including in 2018 [33, 41], in 2019 [47] and in 2024 [46].
Hybridization of the nonlinear CGM has emerged as a significant research direction in optimization science. Recent studies have established strong theoretical foundations for these hybrid methods, demonstrating that they maintain crucial properties such as sufficient descent conditions and convergence under appropriate line search criteria. [1, 4, 5, 8, 16, 22, 24, 29, 32]
Various hybridization techniques that combine the RMIL method with other formulations have been extensively documented in the optimization literature.
For instance, in 2021, Sulaiman et al. [40] introduced a good hybridation of the RMIL and HSM variant, where $\beta_k^{hSM} = \frac{q_k^T (q_k - q_{k-1})}{d_{k-1}^T d_{k-1}} + \frac{2 q_k^T q_{k-1}}{d_{k-1}^T d_{k-1}}$. They established the global convergence under an inexact line searchand applied it to the statistical regression model describing COVID-19.
In 2023, Wahyuningtias [42] proposed another hybrid method combining the RMIL and FR approaches, demonstrating global convergence under Wolfe line search conditions.
On the other hand, there exist many of hybrid CGs based on convex combinations, for example, in 2020, Jardow et al. introduced a notable hybridization of RMIL with MMWU [20], demonstrating promising results in solving large-scale problems.
Recently, Hemici et al. [21] proposed a significant hybrid approach combining RMIL and HS methods, where the

convex parameter θ_k is determined to ensure alignment between the CG direction and the Newton direction.
Similarly, numerous BA-based hybrid conjugate gradient methods using convex combinations approaches that combines the BA and other CGMs, namely the BA–FR [15] hybrid CGM, proposed in 2020. Another notable hybridization, combining the BA and HZ methods, was proposed by BenHanachi et al. in 2025 [9], demonstrating promising results.
Furthermore, Mellal et al. [34] in 2025 developed a new hybrid conjugate gradient algorithm that combines the WYL and BA methods, establishing its global convergence under strong Wolfe conditions and showing improved efficiency on benchmark unconstrained optimization problems.
Some of these hybrid approaches employ the following parameter formulations:

$$\beta_k^{RMILhSM} = \begin{cases} \beta_k^{RMIL} & \text{si } 0 \leq \beta_k^{RMIL} \leq \beta_k^{hSM} \\ \beta_k^{hSM} & \text{ailleurs} \end{cases} [40] \tag{7}$$

$$\beta_k^{RMILFR} = \begin{cases} \beta_k^{RMIL} & \text{si } 0 \leq \beta_k^{RMIL} \leq \beta_k^{FR} \\ \beta_k^{FR} & \text{ailleurs} \end{cases} [42] \tag{8}$$

$$\beta_k^{JN} = \theta_k \beta_k^{MMWU} + (1-\theta_k)\beta_k^{RMIL} [20], \tag{9}$$

$$\beta_k^{HKB} = \theta_k \beta_k^{HS} + (1-\theta_k)\beta_k^{RMIL} [21], \tag{10}$$

$$\beta_k^{BAFR} = \theta_k \beta_k^{BA} + (1-\theta_k)\beta_k^{FR} [15], \tag{11}$$

$$\beta_k^{BAHZ} = \theta_k \beta_k^{HZ} + (1-\theta_k)\beta_k^{BA} [9], \tag{12}$$

$$\beta_k^{BAWYL} = \theta_k \beta_k^{BA} + (1-\theta_k)\beta_k^{WYL} [34], \tag{13}$$

All these formulations preserve the descent property under the strong Wolfe conditions while demonstrating superior numerical performance compared to traditional methods. They maintain sufficient descent properties and guarantee global convergence under appropriate conditions.
To effectively combine the advantages of both BA and RMIL methods and to develop a more efficient and robust algorithm, we introduce a novel hybrid CG method based on a convex combination of these two variants for solving unconstrained optimization problems under suitable conditions.
The combination parameter is carefully chosen to ensure that the resulting search direction is aligned with the Newton direction. The proposed scheme is shown, through rigorous theoretical analysis, to satisfy the sufficient descent property and to achieve global convergence under the strong Wolfe conditions. Using the performance profile of Dolan and Moré, we confirm that our method, denoted as hnBARMIL, consistently outperforms classical (HS, FR, PRP and DY), particularly for large-scale problems.
Furthermore, we demonstrate the practical utility of our method through application to image restoration problems, where hnBARMIL exhibits competitive or superior performance compared to the Fletcher-Reeves algorithm, especially when processing images with higher noise levels. The remainder of this paper is organized as follows: Section 2 presents the novel parameter formulations and outlines the corresponding algorithmic framework. We then provide a comprehensive analysis of the descent properties of the derived search directions, followed by a rigorous proof of their global convergence. Next we present extensive numerical experiments. The final section concludes the paper with a summary of main findings.

2. New hybrid formula

In this part, a newly proposed CGM is introduced. The approach constructs a hybrid CG parameter, $\beta_k^{hnBARMIL}$, as a convex combination of the Al-Bayati & Al-Assady (BA) (5) [2] and Rivaie-Mustafa-Ismail-Leong (RMIL) (6) [38] parameters:

$$\beta_k^{hnBARMIL} = \theta_k \beta_k^{BA} + (1-\theta_k)\beta_k^{RMIL}. \tag{14}$$

Note that θ_k is a scalar parameter bounded by $0 \leq \theta_k \leq 1$.

The search direction $d_{k+1}^{hnBARMIL}$ is defined recursively as:

$$d_{k+1}^{hnBARMIL} = \begin{cases} -q_{k+1}, & \text{for } k = 0, \\ -q_{k+1} + \beta_k^{hnBARMIL} d_k, & \text{for } k \geq 1, \end{cases} \tag{15}$$

where $q_k = \nabla \mathcal{G}(x_k)$ denotes the gradient.
The step size α_k in the iteration $x_{k+1} = x_k + \alpha_k d_k$ is determined using the strong Wolfe (SW) conditions [44, 45]:

$$\begin{aligned} \mathcal{G}(x_k + \alpha_k d_k) &\leq \mathcal{G}(x_k) + \rho \alpha_k q_k^T d_k, \\ |q_{k+1}^T d_k| &\leq \sigma |q_k^T d_k|, \end{aligned} \tag{16}$$

with constants $0 < \rho < \sigma < 1$.
It is evident that, if $\theta_k = 0$ then $\beta_k^{hnBARMIL} = \beta_k^{RMIL}$ and if $\theta_k = 1$ then $\beta_k^{hnBARMIL} = \beta_k^{BA}$.
On the other hand, if $k \geq 1$, then

$$\begin{aligned} d_{k+1}^{hnBARMIL} := -q_{k+1} + \beta_k^{hnBARMIL} d_k &= \theta_k \beta_k^{BA} d_k + -q_{k+1} + (1-\theta_k)\beta_k^{RMIL} d_k \\ &= -q_{k+1} + \theta_k \frac{||y_k||^2}{d_k^T y_k} d_k + (1-\theta_k) \frac{q_{k+1}^T y_k}{\|d_k\|^2}. \end{aligned}$$

In this approach, θ_k is chosen so that the direction $d_{k+1}^{hnBARMIL}$ from (15) coincides with the Newton direction, i.e.,

$$-q_{k+1} + \left[\theta_k \frac{||y_k||^2}{d_k^T y_k} + (1-\theta_k) \frac{q_{k+1}^T y_k}{\| d_k \|^2} \right] d_k = -\nabla^2 \mathcal{G}(x_{k+1})^{-1} q_{k+1} \tag{17}$$

Multiplying both sides of equation (18) by $s_k^T \nabla^2 \mathcal{G}(u_{k+1})$, where $s_k = u_{k+1} - u_k$, we obtain

$$-s_k^T \nabla^2 \mathcal{G}(u_{k+1}) q_{k+1} + \left[\theta_k \frac{||y_k||^2}{d_k^T y_k} + (1-\theta_k) \frac{q_{k+1}^T y_k}{\| d_k \|^2} \right] s_k^T \nabla^2 \mathcal{G}(u_{k+1}) d_k = -s_k^T \nabla^2 \mathcal{G}(u_{k+1}) \nabla^2 \mathcal{G}(x_{k+1})^{-1} q_{k+1} \tag{18}$$

Using the standard secant equation $s_k^T \nabla^2 \mathcal{G}(u_{k+1}) = y_k$, we obtain:

$$-q_{k+1}^T y_k + \left[\theta_k \frac{||y_k||^2}{d_k^T y_k} + (1-\theta_k) \frac{q_{k+1}^T y_k}{\| d_k \|^2} \right] y_k^T d_k = -s_k^T q_{k+1}$$

We have

$$\theta_k \left[\frac{||y_k||^2}{d_k^T y_k} - \frac{q_{k+1}^T y_k}{\| d_k \|^2} \right] y_k^T d_k = -s_k^T q_{k+1} + q_{k+1}^T y_k - \frac{q_{k+1}^T y_k}{\| d_k \|^2} y_k^T d_k$$

which simplifies to:

$$\theta_k^{hn} = \frac{q_{k+1}^T y_k - s_k^T q_{k+1} - \beta_k^{RMIL} (d_k^T y_k)}{(\beta_k^{BA} - \beta_k^{RMIL})(d_k^T y_k)}$$

To ensure numerical stability, we regularize $\theta_k^{hnBARMIL}$ as:

$$\theta_k^{hnBARMIL} = \begin{cases} \theta_k^{hn}, & \text{if } 0 < \theta_k^{hn} < 1, \\ 0, & \text{if } \theta_k^{hn} \leq 0, \\ 1, & \text{if } \theta_k^{hn} \geq 1. \end{cases} \tag{19}$$

Note that, the regularization in equation (19) is essential because when $\theta_k^{hn} \notin [0,1]$, the convex combination property $\beta_k^{hnBARMIL} = \theta_k \beta_k^{BA} + (1-\theta_k)\beta_k^{RMIL}$ breaks down. For $\theta_k^{hn} < 0$, we get negative weight for β_k^{BA} and over weighting of β_k^{RMIL} with $(1-\theta_k) > 1$. For $\theta_k^{hn} > 1$, we obtain negative contribution from β_k^{RMIL} with $(1-\theta_k) < 0$.
Both cases destroy the theoretical foundation ensuring descent properties and convergence guarantees.

3. hnBARMIL ALGORITHM

In this part, we present the hnBARMIL algorithm.

Algorithm 1: hnBARMIL CG Algorithm

Step 1.
Data: Initial point $u_0 \in \mathbb{R}^n$, tolerance $\epsilon > 0$ and $0 < \rho < \sigma < 0.5$.
Calculate $\mathcal{G}(u_0)$ and set $q_0 = \nabla\mathcal{G}(u_0)$. Define $d_0 = -q_0$, put $k = 0$ and go to step 2.
Step 2.
If $\|q_k(u_k)\|_\infty \leq \epsilon$ (Stop creteria), then stop. **Result:** Approximate solution $u^* = u_k$.
Otherwise, go to step 3.
Step 3.
Using SWC (16), calculate the stepsize λ_k, then compute the new iteration $u_{k+1} = u_k + \lambda_k d_k$. Calculate $\mathcal{G}(u_{k+1})$ and put $q_{k+1} = \nabla\mathcal{G}(u_{k+1})$
Step 4. Calculate $\theta_k = \theta_k^{hnBARMIL}$ using (19).
Step 5. Calculate $\beta_k^{hnBARMIL} = \theta_k\beta_k^{BA} + (1-\theta_k)\beta_k^{RMIL}$.
Step 6: : **Restart criterion of Powell** [37] : If $|q_{k+1}^T q_k| \geq 0.2\|q_{k+1}\|^2$ then set $d_{k+1}^{hnBARMIL} = -q_{k+1}$ and $\lambda_{k+1} = 1$, else calculate $d_{k+1}^{hnBARMIL} = -q_{k+1} + \beta_k^{hnBARMIL} d_k$.
Step 7: Put $k = k+1$ and go to Step 2.

4. Convergence Analysis

Global convergence is established by first presenting the following theorem, which proves the sufficient descent of the hnBARMIL direction. In this section, we assume that:

Assumption 1
1) Let

$$\Gamma = \{\, u \in \mathbb{R}^n \mid \mathcal{G}(u) \leq \mathcal{G}(u_1) \,\}$$

be bounded.

2) In some neighborhood N of Γ, $\mathcal{G} \in \mathcal{C}^1$ and q is Lipschitz continuous, i.e.,

$$\exists\, L > 0 \text{ such that } \|q(u_1) - q(u_2)\| \leq L\|u_1 - u_2\|, \quad \forall\, u_1, u_2 \in \Gamma.$$

Under Assumption 1, we obtain :

$$\exists\, B,\ M > 0 : \|u\| \leq B, \qquad and \qquad \|q\,(u)\,\| \leq M, \qquad \forall u \in \Gamma \tag{20}$$

Theorem 1
Under Assumption 1, the direction generated by the hnBARMIL CG algorithm satisfies the sufficient descent condition:

$$q_k^T d_k^{hnBARMIL} \leq -c||q_k||^2,\ \ \forall k\ \geq 0. \tag{21}$$

Proof
We prove this result by mathematical induction.
If $k = 0$, then $q_0^T d_0^{hnBARMIL} = -\|q_0\|^2$, so (21) holds.
On the other hand, for $k > 0$, we have :

$$\begin{aligned} d_{k+1}^{hnBARMIL} &:= -q_{k+1} + \beta_k^{hnBARMIL} d_k \\ &= -q_{k+1} + \left((1-\theta_k)\beta_k^{RMIL} + \theta_k\beta_k^{BA}\right) d_k \\ &= (1-\theta_k)(-q_{k+1} + \beta_k^{RMIL} d_k) + \theta_k(-q_{k+1} + \beta_k^{BA} d_k). \end{aligned}$$

It follows that:

$$d_{k+1}^{hnBARMIL} = (1-\theta_k)d_k^{RMIL} + \theta_k d_k^{BA}.$$

Multiplying by q_{k+1}^T from the left, we get

$$q_{k+1}^T d_{k+1}^{hnBARMIL} = \theta_k q_{k+1}^T d_{k+1}^{BA} + (1-\theta_k)\, q_{k+1}^T d_{k+1}^{RMIL}. \tag{22}$$

When $\theta_k = 0$, the direction $d_k^{hnBARMIL}$ becomes identical to the descent direction of RMIL, yielding:
Firstly, if $\theta_k = 0$ we have :

$$d_{k+1}^{hnBARMIL} = d_{k+1}^{RMIL} = -q_{k+1} + \beta_k^{RMIL} d_k,$$

where they proved in [38] that

$$\begin{aligned} q_{k+1}^T d_{k+1}^{RMIL} &= -q_{k+1}^T q_{k+1} + \beta_k^{RMIL} q_{k+1}^T d_k \\ &= -\left\|q_{k+1}\right\|^2 + \frac{q_{k+1}^T y_k}{\left\| d_k \right\|^2} q_{k+1}^T d_k \\ &\leq -c_1 \left\|q_{k+1}\right\|^2, \text{ for all } k. \end{aligned} \tag{23}$$

Secondly, if $\theta_k = 1$, we have :

$$d_{k+1}^{hnBARMIL} = d_{k+1}^{BA} = -q_{k+1} + \beta_k^{BA} d_k.$$

where they proved in [15] that

$$\begin{aligned} q_{k+1}^T d_{k+1}^{BA} &= -q_{k+1}^T q_{k+1} + \beta_k^{BA} q_{k+1}^T d_k \\ &= -\left\|q_{k+1}\right\|^2 + \frac{||y_k||^2}{d_k^T y_k} q_{k+1}^T d_k \\ &\leq -c_2 \left\|q_{k+1}\right\|^2 \text{ for all } k. \end{aligned} \tag{24}$$

Finally, if $0 < \theta_k < 1$, then :

$$\exists\, \eta_1, \eta_2 \in \mathbb{R} : 0 < \eta_1 \leq \theta_k \leq \eta_2 < 1, \tag{25}$$

From formulas (22) and (25), we conclude

$$q_{k+1}^T d_{k+1}^{hnBARMIL} \leq \eta_1 q_{k+1}^T d_{k+1}^{BA} + (1-\eta_2)\, q_{k+1}^T d_{k+1}^{RMIL},$$

Let $c = \eta_1 c_2 + (1-\eta_2)\, c_1$, then from (23) and (24) we finally get

$$q_{k+1}^T d_{k+1}^{hnBARMIL} \leq -c \left\|q_{k+1}\right\|^2.$$

□

Lemma 1
Under Assumption1, consider any CGM defined by (2) and (3), with step length λ_k determined through the SWL (16). If

$$\sum_{k\geq 0} \frac{1}{\left\|d_k\right\|^2} < \infty,$$

Then

$$\lim_{k\to\infty} \inf \left\|q_k\right\| = 0.$$

Proof
For the proof, refer to [6] . □

Lemma 2
Assuming that Assumption 1 is satisfied, if d_k is a descent direction and λ_k satisfies

$$q_{k+1}^T d_k \geq \sigma q_k^T d_k, : \text{where} : 0 < \sigma < 1,$$

then

$$\lambda_k \geq \frac{(1-\sigma) q_k^T d_k}{L|d_k|^2}. \tag{26}$$

Proof
For the proof of Lemma 2, refer to [30]. □

The following theorem establishes the global convergence properties of our proposed method.

Theorem 2
Consider the hnBARMIL CG algorithm and suppose that assumption 1 holds. Then either $q_k = 0$, for some k, or

$$\lim_{k\to\infty} \inf \|q_k\| = 0. \tag{27}$$

Proof
Consider the hnBARMIL conjugate gradient method and assume that Assumption 1 (1) hold. Suppose that $q_k \neq 0$, for all k. We prove (27) by contradiction. Assume that (27) does not hold, then

$$\exists\, t > 0 : \|q_k\| \geq t,\ \forall\, k, \tag{28}$$

according to the relation (16) and (21), we obtain:

$$q_k^T d_k > c(1-\sigma)\|q_k\|^2 > c(1-\sigma)t^2. \tag{29}$$

By using the Lipschitz condition, we get:

$$\|y_k\| = \|q_{k+1} - q_k\| \leq LB, \tag{30}$$

where $B = \max\{\|u - v\|, u, v \in \Gamma\}$ is the diameter of Γ.
We have

$$d_{k+1}^{hnBARMIL} = -q_{k+1} + \theta_k \beta_k^{BA} d_k + (1-\theta_k)\beta_k^{RMIL} d_k,$$

since, $0 < \theta_k < 1$, we obtain:

$$\|d_{k+1}^{hnBARMIL}\| \leq \|q_{k+1}\| + (|\beta_k^{BA}| + |\beta_k^{hnBARMIL}|)\|d_k\|.$$

We have :

$$\left|\beta_k^{BA}\right| = \frac{||y_k||^2}{\left|d_k^T y_k\right|} \leq \frac{L^2\|s\|^2}{(1-\sigma)ct^2} \leq \frac{L^2 B^2}{(1-\sigma)ct^2}. \tag{31}$$

Otherwise

$$\left|\beta_k^{RMIL}\right| = \frac{g_{k+1}^T y_k}{\|d_k\|^2} \leq \frac{\|g_{k+1}\|\|y_k\|}{\|d_k\|^2} \leq \frac{ML\|s\|^2}{\alpha_k} \leq \frac{MLB^2}{\lambda} \tag{32}$$

Using the above relations (31) and (32), we obtain:

$$\begin{aligned}
\|d_{k+1}^{hnBARMIL}\| \leq \|g_{k+1}\| + (|\beta_k^{BA}| + |\beta_k^{RMIL}|)\|d_k\| &\leq M + (\frac{L^2B^2}{(1-\sigma)ct^2} + \frac{MLB^2}{\lambda})\frac{\|s_k\|}{\lambda} \\
&\leq M + (\frac{L^2B^2}{(1-\sigma)ct^2} + \frac{MLB^2}{\lambda})\frac{B}{\lambda} \\
&\leq \zeta, \quad \text{for all } k
\end{aligned}$$

where

$$\zeta = \frac{M(1-\sigma)ct^2\lambda^2 + LB^2(L\lambda^2 + MB(1-\sigma)ct^2)}{(1-\sigma)ct^2\lambda^2} \tag{33}$$

Thus, we conclude:

$$\sum_{k\geq 0} \frac{1}{\|d_{k+1}^{hnBARMIL}\|^2} = +\infty. \tag{34}$$

By applying Lemma 1, we conclude that:

$$\lim \inf_{k\to\infty} \|g_k\| = 0. \tag{35}$$

This contradicts (28) , and thus we have proved (27) .

□

5. Experimental results

In this part, we report the performance of our hnBARMIL algorithm through two distinct experimental phases.

5.1. Numerical Performance Analysis

The first phase addresses unconstrained optimization problems of the form presented in equation (1).
To assess the effectiveness and convergence characteristics of our hnBARMIL algorithm, we conducted comprehensive numerical experiments on a benchmark suite of 30 well-established test problems drawn from [7, 10] given in table 1 . The evaluation encompasses problems of varying complexity across low, medium, and high dimensions, with problem sizes ranging from $n = 2$ to $n = 10000$.
We compare the performance of our hnBARMIL method against two classes of conjugate gradient algorithms: classical conjugate gradient methods (HS, FR, PRP, and DY) [26, 19, 35, 36, 14] and hybrid conjugate gradient methods (BADY and BAFR) [15], all implemented under the strong Wolfe conditions (16).
The codes are written in Python 3.13 and run on a Lenovo Thinkpad PC with AMD Ryzen 7 PRO 5850U Processor with Radeon Graphics 1.90 GHz and 16.0 GB RAM and Windows 10 Professional 64 bits operating system.
We stop the program when $\|q_k\|_\infty < 10^{-6}$ holds or the number of iterations atteind 5000.
We restart by taking the direction of the steepest descent if either the denominator of β is zero.
We used the parameters values of $\rho = 10^{-4}$ and $\sigma = 0.9$ for the SWC.
we adopt the performance profiles of Dolan and Moré [17] as our primary evaluation metric. This approach provides a comprehensive and statistically robust means of comparing the relative efficiency and reliability of a set of solvers over a collection of benchmark problems. Let S denote the set of solvers, P the set of test problems, n_s the number of solvers, and n_p the number of problems. For each problem $p \in P$ and each solver $s \in S$, let $a_{p,s}$ represent the numerical performance measure of interest, such as the number of iterations or CPU time required to solve problem p with solver s. The performance ratio $r_{p,s}$ for solver s on problem p is defined as:

$$r_{p,s} = \frac{a_{p,s}}{\min\{a_{p,s} : s \in S\}}.$$

By definition, $r_{p,s} \geq 1$ for all p and s, and a value of 1 indicates that solver s achieved the best performance for that particular problem.

The performance profile for solver s is the cumulative distribution function:

$$\sigma_s(\lambda) = \frac{1}{n_p} \left|\{p \in P : r_{p,s} \leq \lambda\}\right|,$$

where $\lambda \geq 1$ is a scaling factor and $\sigma_s(\lambda)$ represents, for each λ, the fraction of problems where the performance ratio of solver s does not exceed λ. When plotted, these profiles visually convey the comparative strengths of the solvers: a curve higher and to the left indicates that the solver was able to solve a larger proportion of problems closer to the best possible performance. Numerical results are compared based on the number of iterations NOI, time CPU and the number of evaluation of the function NFEV and they are given in figures 1

Table 1. List of Test Problems with Initial Points Employed in the Computational Framework

No.	Test Functions	Dimensions	Initial Points
1	Rosenbrock	2, 5, 10	$(-1.2, -1.2)$ for $n = 2$, (1.2,...,1.2) for $n > 2$
2	Sphere	2	(0.5, 0.5)
3	Sum of Squares	2, 5, 10, 100, 1500, 5000, 10000	(1, 1,...,1)
4	Zakharov	2, 5, 10, 100, 1500, 5000, 10000	(1, 1,...,1)
5	Dixon-Price	2, 5, 10, 1500	(2, 2,...,2)
6	Quadratic Function QF1	2, 5, 10, 100, 1000, 1500, 5000	(1, 1,...,1)
7	Raydan 1	2, 5, 10, 100, 1500, 5000	(0.5, 0.5,...,0.5)
8	Raydan 2	2	(1, 1)
9	Extended Rosenbrock	2, 5, 10, 100, 1000, 1500, 5000	(-1.2, -1.2,...,-1.2)
10	Extended DENSCHNF	2, 5, 10, 100, 1000, 1500, 5000	(1, 1,...,1)
11	Extended Tridiagonal	2, 5, 10, 1500	(0, 0,...,0)
12	Extended Himmelblau	2, 5, 10, 100, 1000, 1500	(1, 1,...,1)
13	DBVF	2, 5, 10	(0.1, 0.1,...,0.1)
14	BRYBND	2, 5, 10, 100	(-1, -1,...,-1)
15	Perturbed Quadratic	2, 5, 10, 100	(0.5, 0.5,...,0.5)
16	TRIDIA	2, 5, 10, 100	(1, 1,...,1)
17	Extended Penalty	2, 5, 10, 100, 1000	(1, 1,...,1)
18	BALF	2, 5, 10, 100, 1000	(0.5, 0.5,...,0.5)
19	Diagonal 1	2, 5, 10, 100	(2, 2,...,2)
20	Diagonal 2	2, 5, 10, 100	(2, 2,...,2)
21	Diagonal 3	2, 5, 10, 100, 1000	(0, 0,...,0)
22	Diagonal 4	2, 5, 10, 100, 1000	(1, 1,...,1)
23	Extended Diagonal	100, 1000	(1, 1,...,1)
24	Beale	2, 1500	(1, 1)
25	Booth	2, 1500	(0, 0)
26	Ackley	2, 5, 10	(2, 2,...,2)
27	Rastrigin	2	(1.5, 1.5)
28	Griewank	2, 5, 10	(10, 10,...,10)
29	Matyas	2, 5	(1, 1) for n=2, modified for n¿2
30	Schwefel	2, 5, 10, 1500	(400, 400,...,400)

5.2. Commentaires

In the figures 1, we present the Dolan-Moré performance profiles for five classical conjugate gradient methods: Fletcher-Reeves (FR), Polak-Ribière-Polyak (PRP), Hestenes-Stiefel (HS), and Dai-Yuan (DY), along with hybrid methods BAFR and BADY compared against the proposed hybrid hnBARMIL method. These profiles are generated based on three performance criteria: number of iterations (NOI), CPU time, and number of function evaluations (NFE), evaluated across a comprehensive suite of test functions varying in dimension and computational complexity. The Dolan-Moré performance profiles demonstrate hnBARMIL's clear superiority over all classical conjugate gradient methods (FR, PRP, HS, DY) across the three performance metrics. Specifically, hnBARMIL achieves optimal performance on 65% of problems for iteration count ($\lambda = 1.0$), substantially outperforming HS (60%), PRP (45%), DY (35%), and FR (25%), while maintaining this dominance with 80% efficiency in the critical performance zone ($1.0 \leq \lambda \leq 1.5$). The classical methods FR and HS demonstrate adequate performance for standard problems but exhibit significant degradation as problem complexity and dimensionality increase, particularly evident in the CPU time metric where their curves diverge substantially from hnBARMIL's profile. However, when compared to other hybrid methods BAFR and BADY, hnBARMIL demonstrates competitive performance results with notable distinctions across different problem classes. While BAFR achieves the best overall results due to its superior performance on several benchmark functions including the extended Rosenbrock, Rosenbrock functions.., hnBARMIL exhibits exceptional efficiency on specific test cases, particularly the Zakharov and BRYBND functions. However, this selective performance can be attributed

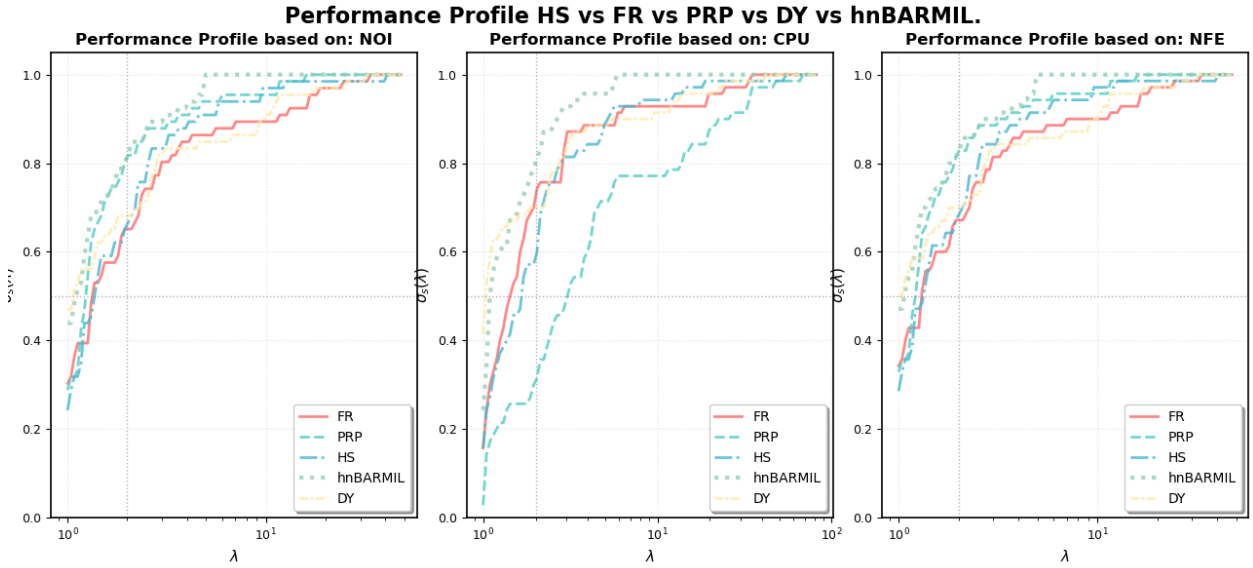

(a) Performance Profile hnBARMIL vs Classical CG

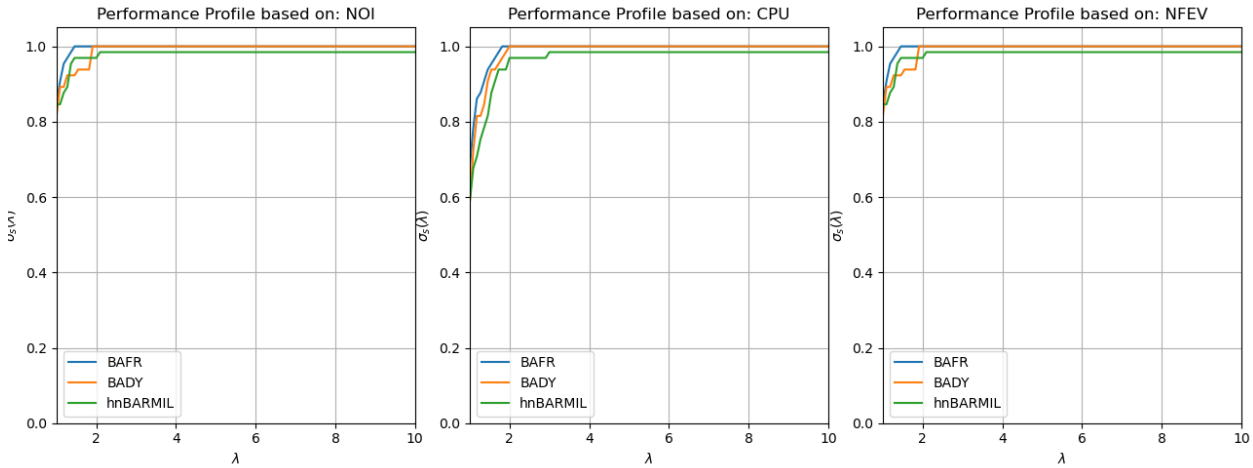

(b) Performance Profile hnBARMIL vs Hybrid CG

Figure 1. Performance Profile of hnBARMIL based on NOI, CPU and NFEV

to a computational drawback in hnBARMIL's theta parameter calculation (conjugacy parameter), which requires expensive inner products between search directions and gradient vectors, potentially increasing computational overhead per iteration. Despite this computational burden, hnBARMIL consistently demonstrates better scalability for large-scale optimization problems, though our experimental evaluation was limited to dimensions up to 10000. The performance advantage of hnBARMIL over hybrid variants is less pronounced than its dominance over classical methods

5.3. Applications of hnBARMIL Algorithm in image restoration

In this section, we employ our proposed hnBARMIL algorithm to solve problem (1), comparing its performance to the FR method. Let ς be an image with dimensions $l_1 \times l_2$, and let $\mathcal{L} = \{1, 2, \ldots, l_1\} \times \{1, 2, \ldots, l_2\}$ represent

the indexing set of the image ς. Let $N \subset \mathcal{L}$ represent the group of noise pixel indices discovered in the first stage. The second step then involves recovering the noise pixels by minimizing $\varsigma(\omega)$:

$$\varsigma_\alpha(\omega) = \sum_{\tau_1,\tau_2 \in N} \left[\omega_{\tau_1,\tau_2} - y_{\tau_1,\tau_2} + \frac{\beta}{2}(2 \times S^1_{\tau_1,\tau_2} + S^2_{\tau_1,\tau_2}) \right]$$

where

$$S^1_{\tau_1,\tau_2} = 2 \sum_{l_1,l_2 \in P_{\tau_1,\tau_2} \cap N^c} \varphi_\alpha(|\omega_{\tau_1,\tau_2} - y_{\tau_1,\tau_2}|), \qquad S^2_{\tau_1,\tau_2} = 2 \sum_{l_1,l_2 \in P_{\tau_1,\tau_2} \cap N} \varphi_\alpha(|\omega_{\tau_1,\tau_2} - y_{\tau_1,\tau_2}|),$$

with $\varphi_\alpha = \sqrt{\alpha + \omega^2}$, $\alpha > 0$, and P represents the collection of the four closest neighbors of the pixel at the specified position. y_{τ_1,τ_2} represents the observed pixel value of the image at position (τ_1, τ_2); see [23, 24, 25, 28]. We use the PSNR, defined by

$$PSNR = 10 \log_{10} \left(\frac{255^2}{\frac{1}{l_1 \times l_2} \sum_{\tau_1,\tau_2} (\omega^k_{\tau_1,\tau_2} - \omega^*_{\tau_1,\tau_2})^2} \right)$$

where $\omega^k_{\tau_1,\tau_2}, \omega^*_{\tau_1,\tau_2}$ denote the pixel values of the restored and original images. We tested Lena (256×256), House (256×256), Elaine (256×256) and Cameraman (256×256). We also set the stopping criteria as

$$\left| \frac{S_\alpha(\omega_k) - S_\alpha(\omega_{k-1})}{S_\alpha(\omega_k)} \right| \leq 10^{-4}.$$

We applied salt-and-pepper noise at three different intensity levels: 50%, 70% *and* 90%.
Figures 2, 3, 4 and 5 display the most notable restoration results for images corrupted at these three noise levels. The data presented in Table (2) has been visualized as a bar chart to enhance the visibility of subtle differences

Table 2. Numerical results for image restoration problem.

Image	Noise level (%)	FR-Method			hnBARMIL-Method		
		NI	NF	PSNR (dB)	NI	NF	PSNR (dB)
Lena	50	82	153	30.5529	31	53	30.5
	70	81	155	27.4824	41	62	27.5264
	90	108	211	22.8583	69	88	22.8453
House	50	52	53	30.6845	27	44	34.9644
	70	63	116	31.2564	37	60	31.1372
	90	111	214	25.2870	41	53	25.2313
Elaine	50	35	36	33.9129	27	38	33.8961
	70	38	39	31.8640	24	35	31.8097
	90	65	114	28.2019	33	49	28.2325
Cameraman	50	59	87	35.5359	28	39	35.4920
	70	78	142	30.6259	33	48	30.7009
	90	121	236	24.3962	50	57	24.9726

between the values. This graphical representation allows for more effective comparison of the results.

The results in Table (2) and the accompanying PSNR plots 6 indicate that the hnBARMIL method not only reduces the number of iterations and computational effort in several cases but also maintains or improves the quality of the restored images, especially at higher noise levels and show the superiority of the hnBARMIL algorithm compared to FR algorithms.

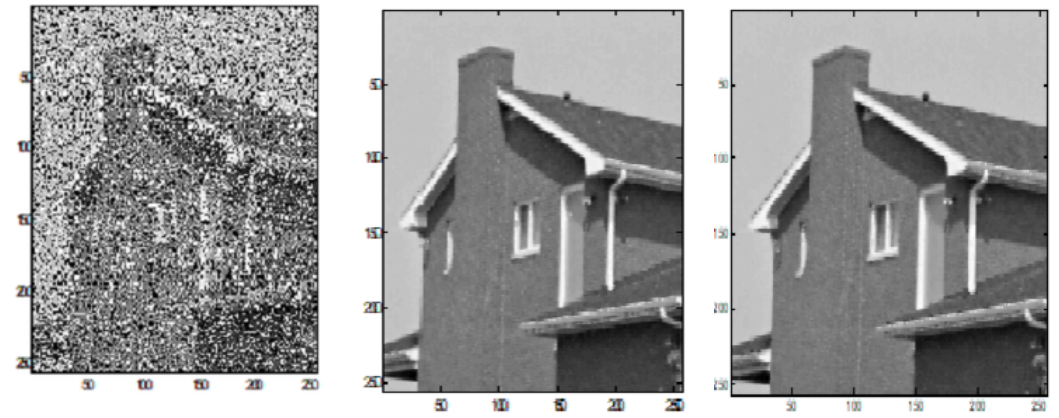

(a) House 50% Noise (b) House 50% FR (c) House 50% hnBARMIL

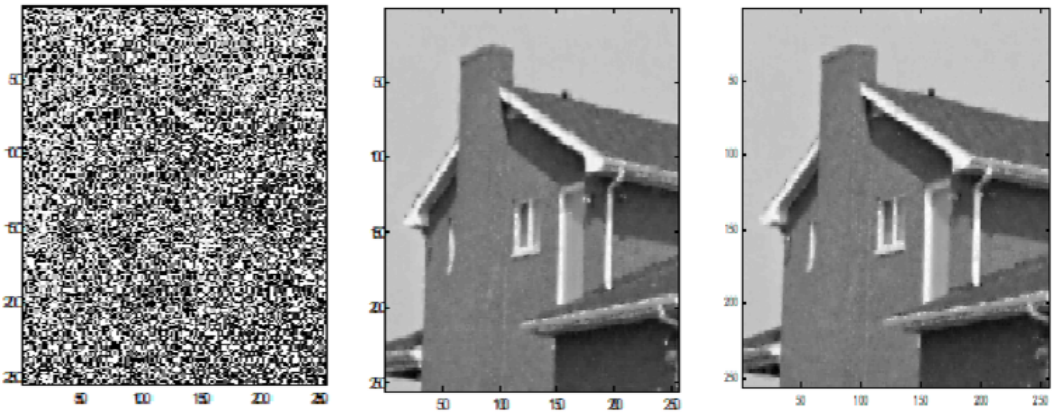

(d) House 70% Noise (e) House 70% FR (f) House 70% HNBARMIL

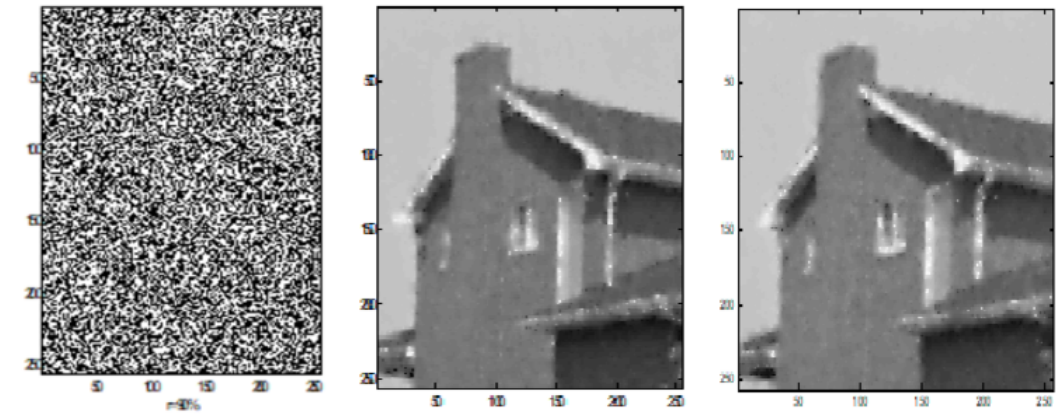

(g) House 90% Noise (h) House 90% FR (i) House 90% hnBARMIL

Figure 2. Restoration of House image corrupted by 50%, 70%, and 90% salt-and-pepper noise using FR and hnBARMIL methods.

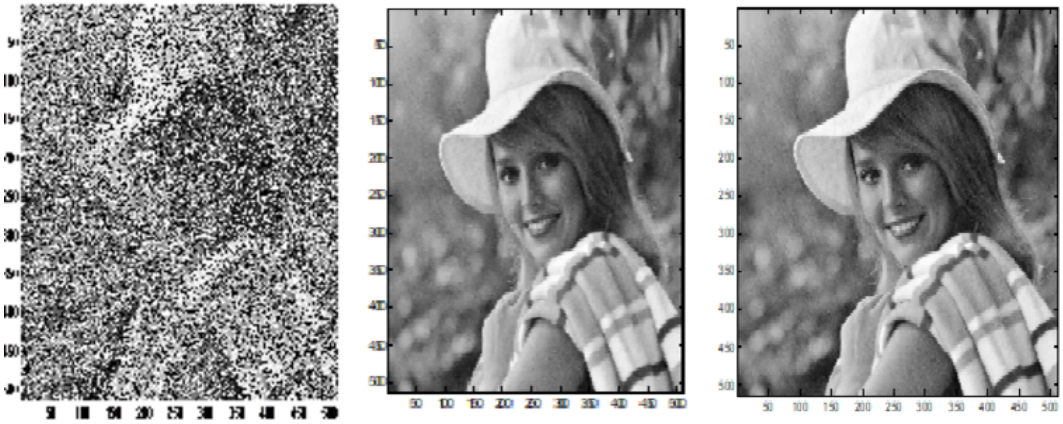

(a) Eleine 50% Noise (b) Eleine 50% FR (c) Eleine 50% hnBARMIL

(d) Eleine 70% Noise (e) Eleine 70% FR (f) Eleine 70% hnBARMIL

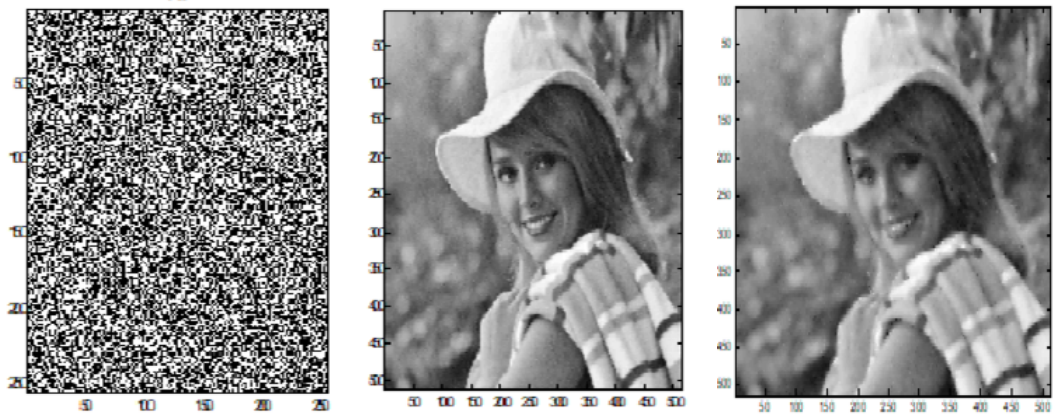

(g) Eleine 90% Noise (h) Eleine 90% FR (i) Eleine 90% hnBARMIL

Figure 3. Restoration of Eleine image corrupted by 50%, 70%, and 90% salt-and-pepper noise using FR and hnBARMIL methods.

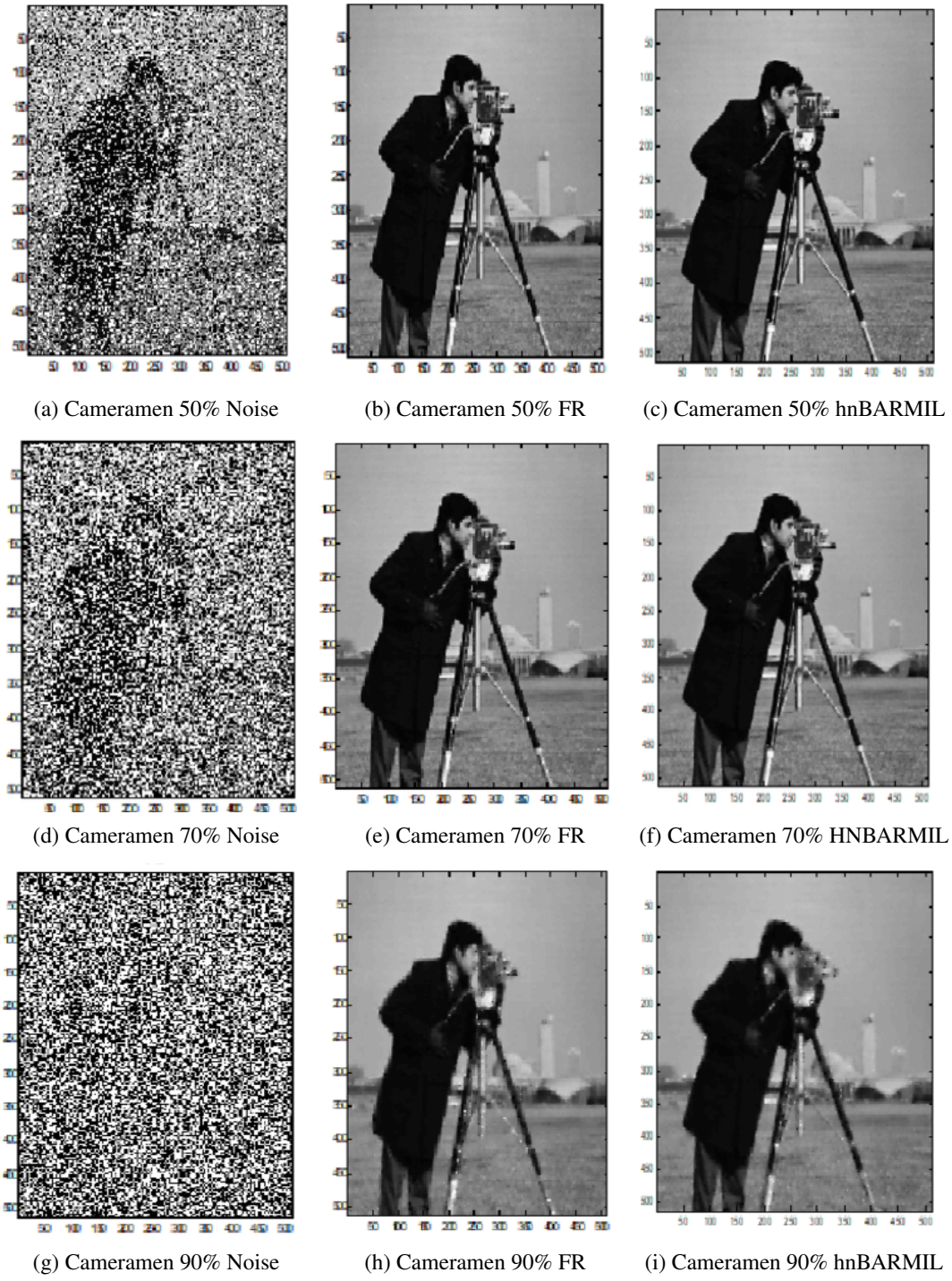

(a) Cameramen 50% Noise (b) Cameramen 50% FR (c) Cameramen 50% hnBARMIL

(d) Cameramen 70% Noise (e) Cameramen 70% FR (f) Cameramen 70% HNBARMIL

(g) Cameramen 90% Noise (h) Cameramen 90% FR (i) Cameramen 90% hnBARMIL

Figure 4. Restoration of Cameramen image corrupted by 50%, 70%, and 90% salt-and-pepper noise using FR and hnBARMIL methods.

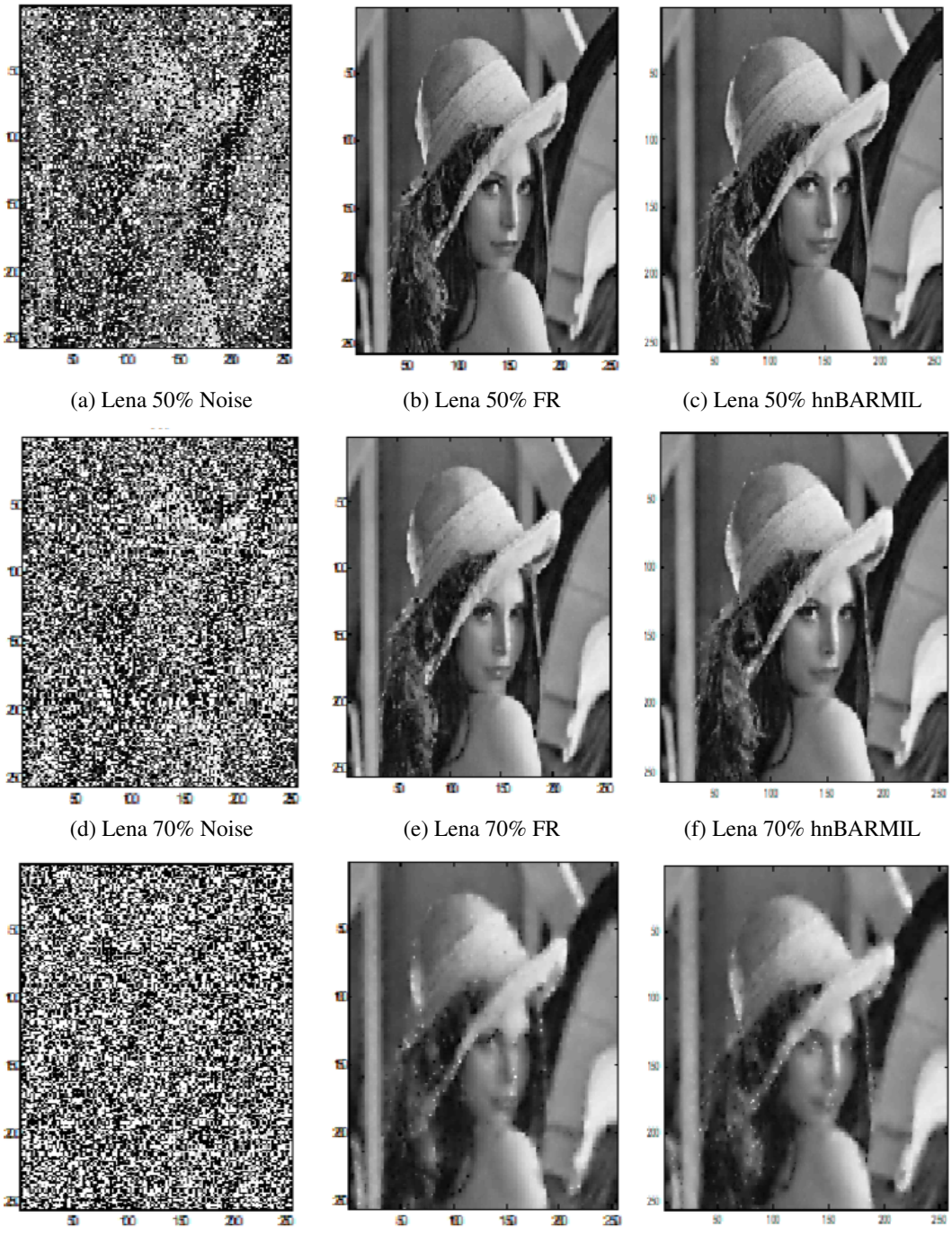

(a) Lena 50% Noise (b) Lena 50% FR (c) Lena 50% hnBARMIL

(d) Lena 70% Noise (e) Lena 70% FR (f) Lena 70% hnBARMIL

(g) Lena 90% Noise (h) Lena 90% FR (i) Lena 90% hnBARMIL

Figure 5. Restoration of Lena image corrupted by 50%, 70%, and 90% salt-and-pepper noise using FR and hnBARMIL methods.

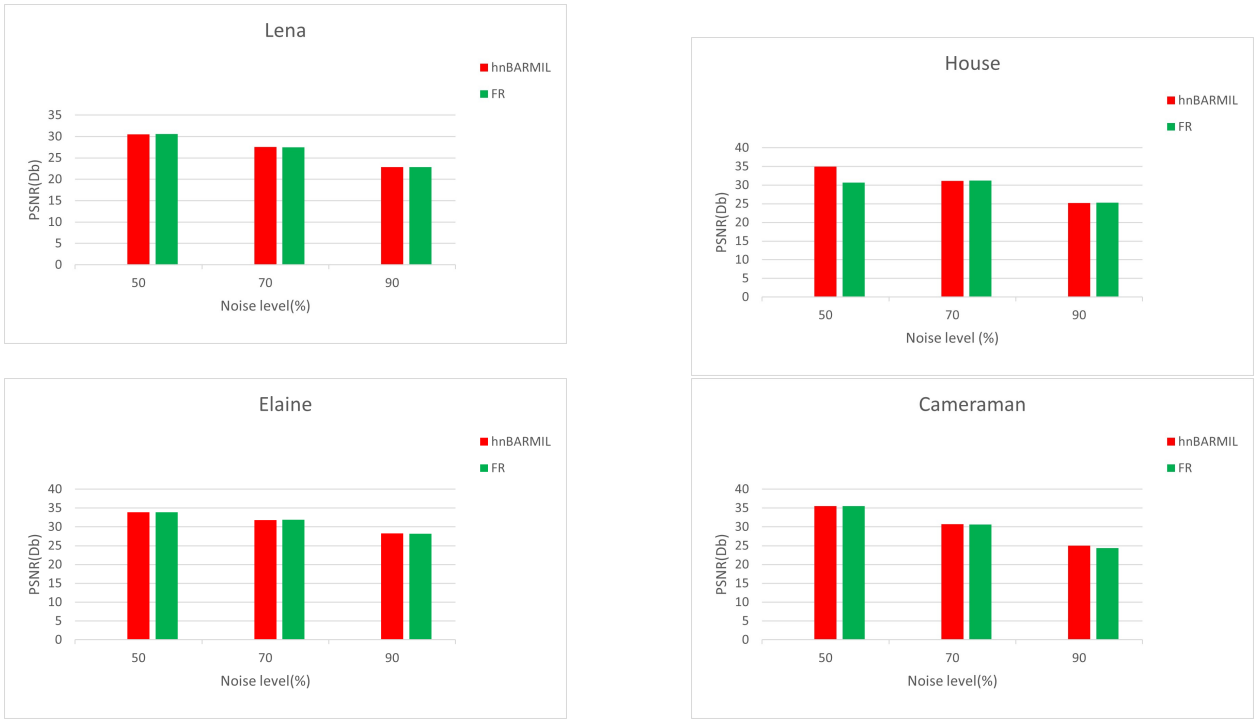

Figure 6. Comparative Analysis of PSNR for hnBARMIL and FR

6. Conclusion

In this work, we have introduced and analyzed a novel hybrid CGM denoted hnBARMIL. The hnBARMIL method is based on a convex combination of the BA and RMIL methods, with its parameter specifically chosen to ensure that the CG direction aligns with the Newton direction. We provided a rigorous convergence analysis under SWC conditions and demonstrated that the proposed algorithm satisfy the sufficient descent property, thereby ensuring global convergence. The Moré-Dolan performance profiles demonstrate hnBARMIL's clear superiority over all classical conjugate gradient methods (FR, PRP, HS, DY) across three performance metrics (NOI, CPU and NFEV). However, when compared to other hybrid methods BAFR and BADY, hnBARMIL shows mixed performance results, with the performance advantage over hybrid variants being less pronounced than its dominance over classical methods. Extensive numerical experiments on the application of image restoration problems, where the hnBARMIL hybrid method is tested on four standard images (Lena, House, Elaine, Cameraman) noised at various intensity levels (50%, 70%, and 90%). The results indicate that the hnBARMIL method not only reduces the number of iterations and computational effort in several cases but also maintains or improves the quality of the restored images, especially at higher noise levels and show the superiority of our algorithm compared to FR algorithm.

REFERENCES

1. D. Ahmed, C. Storey, *Efficient hybrid conjugate gradient techniques*, J. Optim. Theory Appl., 64, 1990.
2. A. Y. Al-Bayati and N. H. Al-Assady, *Conjugate gradient method.*, Tech. Research School of Comp. Studies, Leeds Univ., UK, 1986.
3. A. Y. Al-Bayati and B. A. Hassan, *A new conjugate gradient method for finding the minimum of non linear functions*, Raf. J. of Comp. and Math's. , Vol. 7, No. 1, 2010.

4. S. N. Alsuliman, N. F. Ibrahim, N. A. Hanum Aizam *A new modification of the Wei–Yao–Liu conjugate gradient method for unconstrained optimization and its application in robot control* Journal of Advanced Research in Applied Sciences and Engineering Technology, 314-327, 2024.
5. N. Andrei *Another nonlinear conjugate gradient algorithm for unconstrained optimization* Optim. Meth. Soft., 24, 89–104, 2008.
6. N. Andrei, *Nonlinear conjugate gradient methods for unconstrained optimization*, Springer Optimization and its Applications, Romania, 2020.
7. N. Andrei, *An unconstrained optimization test functions collection*, Adv. Model. Optim. **10** 147–161, 2008.
8. S. Babaie-Kafaki, N. Mirhoseini, and Z. Aminifard, *A Descent Extension of a Modified Polak-Ribiere-Polyak method with application in image restoration problem,* Optimization Letters, vol. 17, no. 2, pp. 351–367, 2023.
9. S. BenHanachi, B. Sellami, M. Belloufi, *Global convergence property with inexact line search for a new conjugate gradient method*, An Inter. Journal of Optimiz. and Control: Theories and Applic. 15, 25-34, 2005.
10. I. Bongartz, A. R. Conn, N. Gould, P. L. Toint, *CUTE: constrained and unconstrained testing environments*, ACM Trans. Math. Soft. **21**, 123–160, 1995.
11. J. F. Cai, R. Chan, B. Morini *Minimization of an edge-preserving regularization functional by conjugate gradient type methods* in Image Processing Based on Partial Differential Equations, Mathematics and Visualization, Springer, Berlin, Heidelberg, 2007.
12. R. H. Chan, C. W. Ho, and M. Nikolova, *Salt-and-pepper noise removal by median-type noise detectors and detail-preserving regularization* IEEE Trans. Image Process., vol. 14, no. 10, pp. 1479-1485, 2005.
13. Z. Dai, *Comment on a New Class of Nonlinear Conjugate Gradient Coefficients with Global Convergence Properties*, Applied Mathematics and Computation, vol. 276, pp. 297-300, 2016.
14. Y. H. Dai, Y. Yuan, *A nonlinear conjugate gradient method with a strong global convergence property*, SIAM J. Optim. , 10, 177-182, 1999.
15. S. Delladji, M. Belloufi, B. Sellami, *New hybrid conjugate gradient method as a convex combination of FR and BA methods*, J. Inform. Optim. Sci., 42, 591-602, 2021.
16. S. Djordjevic, *New hybrid conjugate gradient method as a convex combination of HS and FR*, Journal of Applied Mathematics and Computation, 9, 366-378, 2018.
17. E. D. Dolan, J. J. Moré, *Benchmarking optimization software with performance profiles*, Math. Program. **91**, 201-213, 2002.
18. R. Fletcher, *Practical Methods of Optimization. Unconstrained Optimization*, Wiley, New York, 1987.
19. R. Fletcher, C. M. Reeves, *Function minimization by conjugate gradients*, Comput. J. ,7, 149-154, 1964.
20. F. N. Jardow, G. M. Al-Naemi, A new hybrid conjugate gradient algorithm for unconstrained optimization with inexact line search Indon. J. Elec. Eng. Comput. Sci. 20, 939–947, 2020.
21. Y. E. Hemici, S. Khelladi, D. Benterki, New hybrid conjugate gradient method for nonlinear optimization with application to image restoration problems Kybernetika, 60, 535–552, 2024.
22. I. Guefassa, Y. Chaib and T. Bechouat *Another hybrid conjugate gradient method as a convex combination of WYL and CD methods*, Monte Carlo Methods and Applications, vol. 30, no. 3, pp. 225-234, 2024.
23. B. A. Hassan and H. A. Alashoor, *On image restoration problems using new conjugate gradient methods* Indonesian Journal of Electrical Engineering and Computer Science, vol. 29, no. 3, pp. 1438-1445, 2023.
24. B. A. Hassan and H. M. Sadiq, *Efficient New Conjugate Gradient Methods for Removing Impulse Noise Images,* European Journal of Pure and Applied Mathematics, vol. 15, no. 4, pp. 2011-2021, 2022.
25. B. A. Hassan, Y. A. Mohamm *Innovative conjugate gradient method for image impulse noise* Journal of Interdisciplinary Mathematics, vol. 28, no. 1, pp. 347-353, 2025.
26. M. R. Hestenes, E. Stiefel, *Methods of conjugate gradients for solving linear systems*, J. Res. Natl. Bur. Stand., 49, 409-436, 1952.
27. A. L. Ibrahim, B. G. Fathi and M. B. Abdulrazzaq *Conjugate gradient techniques: Enhancing optimization efficiency for large-scale problems and image restoration*, Numerical Algebra, Control and Optimization, 15, 4, 1151-1175, 2025.
28. H. M. Khudhur, B. A. Hassan, and S. Aji *Superior formula for gradient impulse noise reduction from images*, International Journal of Applied and Computational Mathematics, vol. 10, no. 1, p. 4, 2024.
29. X. Li *A hybrid Polak–Ribière–Polyak and Wei–Yao–Liu conjugate gradient method for unconstrained optimization* Journal of Inequalities and Applications, 2019.
30. J. K. Liu and S. J. Li, *New hybrid conjugate gradient method for unconstrained optimization.* Applied Mathematics and Computation, 245, 36-43, 2014.
31. Y. Liu, C. Storey, *Efficient generalized conjugate gradient algorithm. Part 1: Theory*, J. Optim. Theory Appl. , 69, 129-137, 1991.
32. W. Liu, Z. Wei, L. Liu *A new hybrid conjugate gradient method for multiobjective optimization* Abstract and Applied Analysis, 2014.
33. A. V. Mandara, M. Mamat, M. Waziri, M. A. Mohamed, U. A. Yakubu, *A new conjugate gradient coefficient with exact line search for unconstrained optimization* Far East Journal of Mathematical Sciences, vol. 105, pp. 193–206, 2018.
34. R. Mellal and N. Sellami *A Novel Hybrid Conjugate Gradient Algorithm for Solving Unconstrained Optimization Problems.* Statistics, Optimization and Information Computing, 2025, https://doi.org/10.19139/soic-2310-5070-2807.
35. E. Polak, G. Ribiere, *Note sur la convergence des méthodes de directions conjuguées*, Rev. Française Inform. Recherche Opertionelle, 16, 35-43, 1969.
36. B. T. Polyak, *The conjugate gradient method in extreme problems*, U.S.S.R. Comput. Math. Phys. , 9, 94-112, 1969.
37. M. J. D. Powell, *Restart procedures of the conjugate gradient method*, Math. Program. **2**, 241–254, 1977.
38. M. Rivaie, M. Mustafa, W. J. Leong, M. Ismail, *A new class of nonlinear conjugate gradient coefficients with global convergence properties*, Appl. Math. Comput. 218, 11323-11332, 2012.
39. M. Rivaiea, M. Mamat, b. A. Abashar, *A new class of nonlinear conjugate gradient coefficients with exact and inexact lines earches* Applied Mathematics and Computation, V.268, 1152–1163, 2015.
40. I. M. Sulaiman, N. Abu Bakar, M. Mamat, B. A. Hassan, M. Malik, A. M. Ahmed *A new hybrid conjugate gradient algorithm for optimization models and its application to regression analysis* Indonesian Journal of Electrical Engineering and Computer Science, Vol. 23, No. 2, pp. 1100-1109, 2021.

41. I. Sulaiman, M. Waziri, E. Olowo, A. Talat, *Solving fuzzy nonlinear equations with a new class of conjugate gradient method* Malaysian Journal of Computing and Applied Mathematics, vol. 1, no. 1, pp. 11–19, 2018.
42. L. D. R. Wahyuningtias *Global Convergence of Modified RMIL Parameter in Conjugate Gradient Method* Volume 31, Issue 3, Engineering Letters, 2023.
43. Z. Wei, S. Yao, L. Liu *A new conjugate gradient method for unconstrained optimization* Applied Mathematics and Computation, 2006.
44. P. Wolfe, *Convergence conditions for ascent methods*, SIAM Rev., 11, 226-235, 1969.
45. P. Wolfe, *Convergence conditions for ascent methods. II: Some corrections*, SIAM Rev. 13, 185-188, 1971.
46. O. O. O. Yousif and M. A. Saleh, *Another modified version of RMIL conjugate gradient method*, Applied Numerical Mathematics, V:202, pp. 120-126, 2024.
47. M. B. Yousef, M. Mamat, and M. Rivaie, *A new modified RMIL cg method with global convergence properties* Conference Proceedings, AIP Publishing LLC, vol. 2184, p. 60-50, 2019.